# BREMSTRAHLUNG AND ION BEAM CURRENT MEASUREMENTS WITH SuSI ECR ION SOURCE *

T. Ropponen†, D. Cole, G. Machicoane, A. Stolz, L. T. Sun, L. Tobos
National Superconducting Cyclotron Laboratory, Michigan State University

*Abstract*

The Superconducting Source for Ions (SuSI) [1] at the National Superconducting Cyclotron Laboratory at Michigan State University is a fully superconducting 3rd generation ECR ion source currently operated with two 18 GHz klystrons. The axial magnetic field is generated by six solenoid magnets which allow to control the magnetic field characteristics, such as resonance locations, mirror ratios and magnetic field gradients, almost independently. In this paper we will focus on the measurements done with different collimation geometries and we will show results comparing FlatB and normal Bmin operation. We will also discuss about the effect of different magnetic field gradients while keeping the length of the plasma and value of $B_{min}$ as constants.

## MEASUREMENT SETUP AND MAGNETIC FIELD PROFILES

The bremsstrahlung measurements presented in this paper are steady state high energy measurements. The bremsstrahlung events were recorded axially through the diagnostic port of the analyzing magnet using an Ortec p-type germanium detector. A small solid angle for the detection of bremsstrahlung was achieved using two collimators separated by 445 mm. Each collimator was made of lead for the outer parts and tungsten for the inserts. The layout of the collimator structure is presented in figure 1. The area at the extraction aperture of SuSI that was seen by the detector was about ⌀ 7 mm while SuSI plasma electrode has an opening of ⌀ 10 mm. In addition to these two collimators the existing lead shielding in the ECR area was put to use in order to decrease the amount of scattered radiation. First, a stand-alone lead shielding plate (25 mm of Pb, 6 mm of steel) positioned between the two collimators was used during the measurements. Second, the ECR area is confined using several large lead panels (13 mm of lead, 6 mm of steel) and one was positioned between the second collimator and the Ge detector. A 5 mm hole was drilled through both the shielding plate and the lead wall panel to allow the radiation to reach the detector. The distance from the plasma electrode to the detector was about 3.2 m. Figure 2 presents the general layout of the measurement setup.

The collimators were aligned through the injection flange using a laser and $^{133}$Ba and $^{152}$Eu sources were used for energy and relative efficiency calibration. Energy resolution of the setup was 2.14 keV at 80.997 keV, 2.97 keV at 443.965 keV and 6.15 keV at 1085.842 keV. Measurement time was fixed to 30 min per set and typical count rates at the detector varied between 2 kHz and 75 kHz. Background radiation has been subtracted from the data presented in this paper.

The measurements were conducted using analog NIM, CAMAC and VME electronics. The electronics is divided into two branches — the so-called slow branch for energy and the fast branch for timing information. Due to this arrangement, the system is capable of detecting pile-up events. Shaping time of the linear amplifier was set to 3 $\mu$s and the signal width was roughly 6 $\mu$s. When two or more

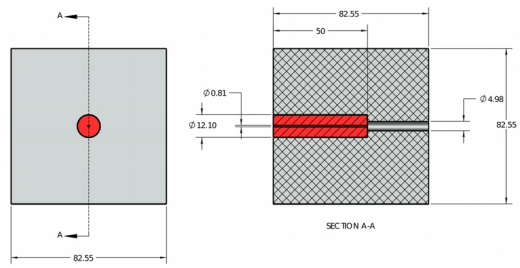


Figure 1: Cross-section view of the collimator structure. Both collimators that were used in the setup are identical. Lead is marked with gray color and tungsten insert with red. Dimensions are given in inches.

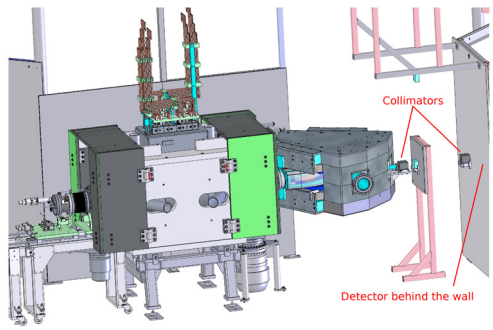


Figure 2: Layout of the measurement geometry. The first collimator is located next to the bending magnet flange (glass window) and the second one is attached to the ECRIS room wall. The stand-alone Pb shield is seen between the collimators. The detector was located behind the wall and was shielded with Pb blocks in order to decrease the background levels.

* This work was supported by the National Science Foundation under Grant No. PHY-0110253
† ropponen@nscl.msu.edu

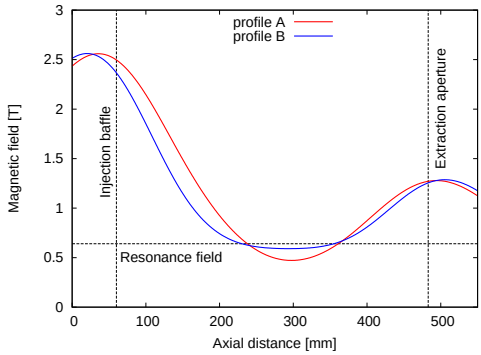


Figure 3: Magnetic field profiles for flatB and normal Bmin operation. See table 1 for details. Note that there is a difference of 0.1 T in the magnetic field at the injection baffle position.

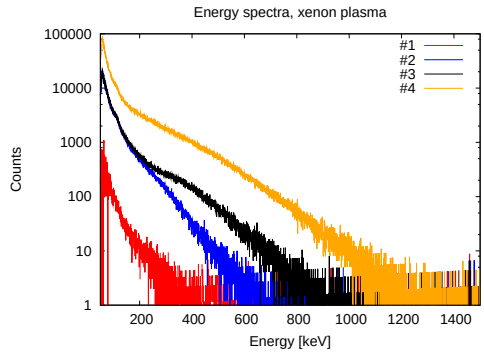


Figure 4: Energy spectra with different collimation geometries: #1 all collimators, #2 collimator at the dipole is removed, #3 Collimator at the dipole, Pb blocks inside the dipole and the stand-alone Pb shield are removed, #4 all the collimating elements except the Pb wall are removed. See also fig. 2.

Table 1: Axial magnetic field profile details. Resonance locations are given in same coordinates that are used in figure 3.

| #profile | gradB (inj, ext) | plasma length | res. location (inj, ext) |
|---|---|---|---|
| A | -5.73 T/m, 5.01 T/m | 124.5 mm | 237.3 mm, 361.8 mm |
| B | -2.19 T/m, 2.25 T/m | 127.1 mm | 229.1 mm, 356.1 mm |
| C | -5.19 T/m, 4.75 T/m | 125.4 mm | 237.8 mm, 363.2 mm |
| D | -6.38 T/m, 5.39 T/m | 124.3 mm | 236.1 mm, 360.4 mm |

events were observed within 20 $\mu$s they were considered to be pile-up events. The charge state distributions (CSDs) were recorded after the SuSI collimation channel [2].

For the FlatB measurements described in this paper we used the magnetic field profiles shown in figure 3. Field profile #A is used as a reference field and it is a starting point to normal operation with SuSI while producing medium charge states at 18 GHz. Position of the injection baffle, which was kept as constant during the measurements, the extraction aperture position and the resonance field for 18 GHz is marked in these figures. Value of 0 mm refers to the location of the entrance face of the first solenoid. The details of the profiles can be seen in table 1. The radial field was kept constant between measurement sets.

## DIFFERENT COLLIMATION SCHEMES

The collimation scheme that was used in the measurements limits the area that the detector sees within the extraction aperture of SuSI. This means that we were mostly measuring radiation coming directly from the plasma processes and also some back-scattered radiation from the injection. We studied the effect of different collimation schemes and removed the collimators and additional shielding one-by-one increasing the area which the detector can observe. Energy spectra from this study, recorded using 1200 W of RF power and magnetic field profile #A, is presented in figure 4. The diameters of the circular areas at the extraction aperture position seen by the detector are roughly the following #1: 7 mm, #2: 62 mm, #3: 83 mm and #4: 4.7 m. It is noted that with collimation #4 the solid angle defined only by the hole in the Pb wall exceeds the size of the Ge crystal significantly at the location of the detector. Thus, the detector cannot observe all the radiation coming through the aperture. The endpoint energies presented in this paper are estimated by the eye due to the difficulties of obtaining endpoint energy from measurement data that is not entirely linear even at logarithmic scale.

With collimation #1, when the detector sees only the plasma, the endpoint energy of the spectrum lies a bit lower than 400 keV. With #2 we are observing roughly 650 keV and with #3 the endpoint energy is about 850 keV. When the last movable collimator is removed the endpoint energy rises to around 1200 keV. The difference between #1 and #2 is clearly the difference between just the plasma bremsstrahlung and the bremsstrahlung coming from the plasma and from the high energy electron losses towards the extraction. The difference between #2 and #3 is assumed to originate from the decreased shielding for scattered high energy radiation. With #4 the effect of collimation is almost non-existent and detector records both high count rates and energies over 1 MeV. It is clear, that the effect of the different collimation schemes is significant. Thus, if only the plasma bremsstrahlung is wanted to be studied a very tight collimation (within the extraction aperture) must be used. Comparing #2 and #3 reveals also the well-known issue concerning the impact of the scattered radiation on the shape of the spectrum.

In figure 5 the data from #4 is presented with and without efficiency correction and pile-up rejection. It is seen that the efficiency calibration has a clear impact on the shape of the low energy (0–120 keV) part and a smaller, but noteworthy, impact on the high energy (300 keV and higher) part of the spectrum. The efficiency calibration can thus

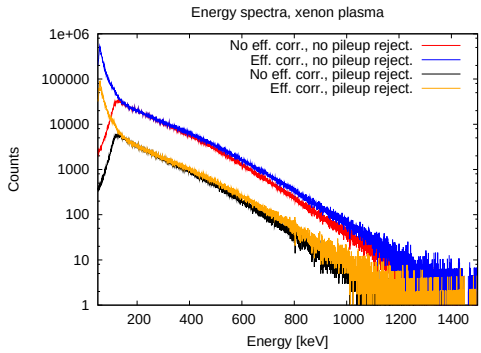


Figure 5: Energy spectra #4 (see fig. 4) with and without detector efficiency calibration and pile-up rejection.

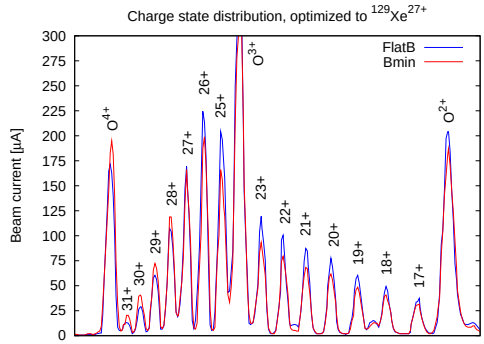


Figure 6: Xenon charge state distribution with normal B-min (profile #A) and Flat-B (profile #B) magnetic field profiles.

affect for example estimates for endpoint energies and values for spectral temperature (see table 2). The pile-up rejection does not seem to have such a clear impact on the slope i.e. spectral temperature but the endpoint energy can change significantly. In the case of this example (fig. 5), the endpoint energies change roughly from 1430 keV to about 1230 keV when the pile-up rejection is applied. Similar change (around 65 keV) is also observed with #1 (data not presented here). Count rates for background and measurement #1 were comparable, which means that pile-up rejection can be important also at low count rates.

## FLATB VS. BMIN OPERATION

By tuning the SuSI magnetic field to very low gradients one has to accept the change of axial length of the plasma and $B_{min}$ (see fig. 3). During this study the plasma length was varied from 124.5 mm to 127.1 mm with magnetic field profiles #A and #B, respectively. SuSI is capable of generating even lower gradient field profiles, but we choose not to use such a profile due to extremely high radiation levels. While the radiation monitor observing X-rays at the SuSI's extraction reported 6.1 mR/h with B-field profile #A (1500 W/18.0 GHz + 350 W/17.8 GHz) the level went up to 50 mR/h with profile #B with the same RF powers. When we tested a profile with even lower magnetic field gradient (0.79 T/m both injection and extraction) the radiation levels exceeded 31 mR/h already at 700 W. In addition to high radiation levels, it was observed that the plasma was very unstable and the source very sensitive to tuning, compared to normal Bmin operation, whenever a FlatB profile was used.

The charge state distributions of xenon plasma with oxygen as a support gas are presented in figure 6 and the corresponding bremsstrahlung spectra are shown in figure 7. It was found out that similar amounts of $^{129}Xe^{27+}$ beam current could be extracted when SuSI was tuned to $Xe^{27+}$ with both profiles keeping the RF power constant. From the CSD it can be seen that during the FlatB operation slightly more low and medium charge states but less high charge

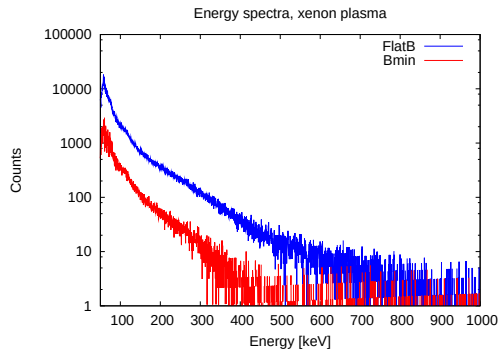


Figure 7: Energy spectra with normal Bmin (profile #A) and FlatB (profile #B) magnetic field profiles.

states are observed compared to Bmin operation. The difference can arise from the difference in the injection magnetic field (a slightly lower confinement with FlatB operation, see fig. 3) or from the magnetic field profile/gradient (differences in electron energy distribution). During the measurements the drain current of the source was relatively constant (4.4 mA and 4.5 mA with FlatB and Bmin, respectively) and the leak valve setting ratio between xenon and oxygen feed was 0.75 in both cases meaning that the gas mixing ratio was not playing a major part on the shape of the CSDs. Extraction pressures of 8.2e-8 and 9.5e-8 torr were recorded with FlatB and Bmin, respectively. By looking at the bremsstrahlung emission from figure 7 it is clear that the FlatB operation produces both higher count rates and significantly higher endpoint energies. It can be estimated that with FlatB operation the endpoint energies are in the area of 850 keV while with the normal Bmin operation the energies are below 450 keV. While the 2 mm Ta shield used around SuSI plasma chamber can decrease the radiation load of less than 400 keV photons effectively, it becomes more transparent to higher energies which are plenty in the FlatB operation. See table 2 for spectral temperatures.

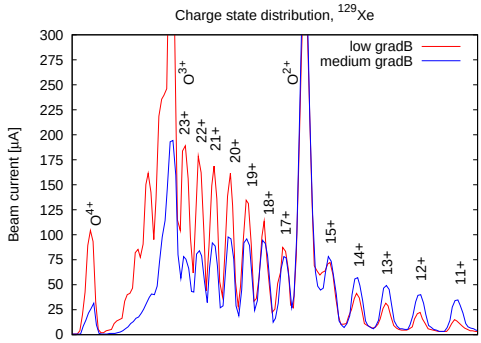


Figure 8: Xenon charge state distribution with different magnetic field gradients.

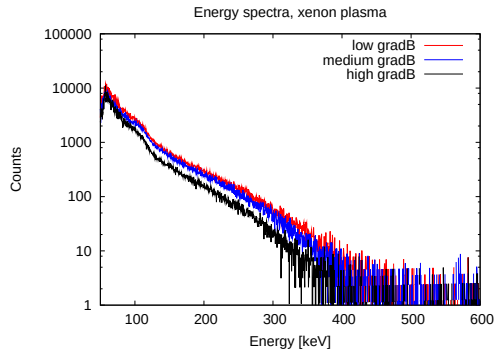


Figure 9: Energy spectra with different magnetic field gradients.

## DIFFERENT GRADIENTS WITH FIXED PLASMA LENGTH AND $B_{MIN}$

The magnetic field gradient in the resonance zone can be tuned in SuSI within certain limits while other field characteristics are kept almost fixed. Plasma length varies only 1.1 mm between the different profiles and the maximum deviation in the $B_{min}$ is 0.039 T. The ion source was tuned to $^{129}Xe^{20+}$ using the medium gradient (profile #A) and 1500 W of RF power. The source settings other than the magnetic field profile were not changed while using low (profile #C) and high (profile #D) gradient profiles.

The CDSs for medium and low gradient are shown in figure 8 where it can be seen that while the CSD is peaked at 20+ with the medium gradient profile the CSD is significantly different and peaking at 23+ when the gradient is lowered. Beam currents of charge states higher than 17+ are clearly increased and the beam intensity at 23+ is roughly 2.5 times higher. Drain currents were 5.0 mA in both cases and extraction pressures of 1.6e-7 and 1.4e-7 torr were recorded with medium and low gradient profiles, respectively. This suggests that while the source settings were kept relatively constant only very small changes in the magnetic field gradient can create significantly different plasma conditions.

Figure 9 shows that the count rates at the low energy part are roughly similar while there is a clear difference above 75 keV. The endpoint energies are 405 keV, 435 keV and 470 keV for high, medium and low gradient, respectively. For spectral temperatures, see table 2. As previously has been observed (see e.g. [3, 4]), the lower the gradient the higher the count rate, the endpoint energy and the spectral temperature. With these previous measurements the change in the magnetic field gradient also meant changing the $B_{min}$ and length of the plasma. Because the length of the plasma and value of $B_{min}$ were kept roughly constants in our measurements, it is experimentally confirmed for the first time that the value of the magnetic field gradient alone plays a major role especially in the ion beam and also in the radiation production.

## DISCUSSION AND CONCLUSIONS

In the measurement described in this paper we have presented the importance of the efficiency correction and pile-up rejection event at very low count rates. We have also shown that while the FlatB operation can produce similar ion beam currents than normal Bmin operation, the radiation levels and photon energies are significantly higher if FlatB mode is used. This results into higher heat loads to cryostat systems. We also demonstrated that a slight change in the magnetic field gradient can significantly change the ion beam production when the length of the plasma and $B_{min}$ are not changed. These observations favor constructing ECR ion sources with flexible axial magnetic field structures found at the moment only in SuSI and in SC-ECRIS in Riken [5].

Table 2: Spectral temperatures and endpoint energies [keV] for the different measurements. Fitting ranges for spectral temperatures are given in each section of the table.

different collimations, #4 (fig. 5) (fit range 600–800 keV)

| no eff. corr. no pile-up reject. | eff. corr. no pile-up reject. | no eff. corr. pile-up reject. | eff. corr. pile-up reject. |
|---|---|---|---|
| 118.9±0.6 | 129.9±0.7 | 117.7±1.3 | 128.5±1.5 |
| 1340±30 | 1430±30 | 1140±30 | 1230±30 |

| FlatB vs. Bmin (fig. 7) (fit range 130–200 keV) | | gradB (fig. 9) (fit range 130–200 keV) | | |
|---|---|---|---|---|
| FlatB | Bmin | low gradB | medium gradB | high gradB |
| 68.1±1.1 | 58.0±1.7 | 60.1±0.9 | 57.8±0.8 | 56.4±0.9 |
| 850±20 | 450±20 | 470±20 | 435±20 | 405±20 |

## REFERENCES

[1] P. A. Zavodszky *et al.* Rev. Sci. Instrum. 77, 03A334 (2006).

[2] G. Machicoane *et al.* Conference presentation, ICIS2009 (2009).

[3] D. Leitner *et al.* Rev. Sci. Instrum. 79, 033302 (2008).

[4] T. Ropponen *et al.* Nucl. Instr. and Meth. A 600, p. 525–533 (2009).

[5] T. Nakagawa *et al.* Rev. Sci. Instrum. 81, 02A320 (2010).